JOURNAL OF GEOPHYSICAL RESEARCH, VOL. 101, NO. E4, PAGES 9227–9237, APRIL 25, 1996

Detection and monitoring of H_2O and CO_2 ice clouds on Mars

James F. Bell III,[1] Wendy M. Calvin,[2] Maureen E. Ockert-Bell,[1] David Crisp,[3]
James B. Pollack,[4,5] and John Spencer[6]

Abstract. We have developed an observational scheme for the detection and discrimination of Mars atmospheric H_2O and CO_2 clouds using ground-based instruments in the near infrared. We report the results of our cloud detection and characterization study using Mars near IR images obtained during the 1990 and 1993 oppositions. We focused on specific wavelengths that have the potential, based on previous laboratory studies of H_2O and CO_2 ices, of yielding the greatest degree of cloud detectability and compositional discriminability. We have detected and mapped absorption features at some of these wavelengths in both the northern and southern polar regions of Mars. Compositional information on the nature of these absorption features was derived from comparisons with laboratory ice spectra and with a simplified radiative transfer model of a CO_2 ice cloud overlying a bright surface. Our results indicate that both H_2O and CO_2 ices can be detected and distinguished in the polar hood clouds. The region near 3.00 μm is most useful for the detection of water ice clouds because there is a strong H_2O ice absorption at this wavelength but only a weak CO_2 ice band. The region near 3.33 μm is most useful for the detection of CO_2 ice clouds because there is a strong, relatively narrow CO_2 ice band at this wavelength but only broad "continuum" H_2O ice absorption. Weaker features near 2.30 μm could arise from CO_2 ice at coarse grain sizes, or surface/dust minerals. Narrow features near 2.00 μm, which could potentially be very diagnostic of CO_2 ice clouds, suffer from contamination by Mars atmospheric CO_2 absorptions and are difficult to interpret because of the rather poor knowledge of surface elevation at high latitudes. These results indicate that future ground-based, Earth-orbital, and spacecraft studies over a more extended span of the seasonal cycle should yield substantial information on the style and timing of volatile transport on Mars, as well as a more detailed understanding of the role of CO_2 condensation in the polar heat budget.

Introduction and Background

Mars has a dynamic seasonal cycle of carbon dioxide exchange between the surface and the atmosphere. CO_2 is the dominant atmospheric component, and thus changes in solar insolation which affect CO_2 have global consequences. Because of its Earth-like obliquity, the Martian polar regions go through long periods of zero solar insolation. The winter polar temperatures decrease until they reach the CO_2 condensation temperature (≈150 K), and a large fraction of the atmosphere (≈25% as measured during the Viking mission [*Zurek et al.*, 1992]) condenses as polar caps. As insolation returns to the polar regions, the process is reversed as the CO_2 ice stored in the polar cap sublimes. This condensation cycle between the surface and the atmosphere effectively determines the minimum surface temperature of the planet, and variations in the rate and/or amount of CO_2 condensation or sublimation, in concert with the interrelated cycles of water and dust on Mars, have important consequences for the climate (e.g., see reviews by *James et al.* [1992], *Jakosky and Haberle* [1992] and *Kahn et al.* [1992]).

In addition to atmospheric vapor and surface ice, there are two additional reservoirs for the storage of CO_2 during the Mars seasonal cycle. The first is the regolith [e.g., *Fanale and Cannon*, 1974], which could serve as a long-term sink of CO_2 in carbonate rocks or through adsorption [e.g., *Kahn*, 1985; *Fanale et al.*, 1992 and references therein]. There have been (and still are) significant observational and theoretical efforts to try to detect carbonates and other salts on Mars to find evidence of a possible early, thick CO_2 atmosphere [e.g., *Pollack et al.*, 1987, 1990a; *Blaney and McCord*, 1989; *Clark et al.*, 1990; *Gooding*, 1992; *Bell and Crisp*, 1993].

The second alternate reservoir is CO_2 clouds, which might play a role in the CO_2 condensation cycle. *Geirasch and Goody* [1968] performed a theoretical study of CO_2 clouds that indicated that CO_2 cloud condensation was unlikely on Mars except possibly during polar night. This finding was supported by early general circulation model (GCM) calculations [e.g., *Leovy and Mintz*, 1969] that predicted atmospheric temperatures too high for CO_2 cloud condensation. These results were used to support the contention that the Mars winter polar hood clouds seen in telescopic and spacecraft images are primarily composed of water ice. *Pollack et al.* [1981] performed more detailed GCM calculations that included topographic effects but that did not explicitly include condensation. Their model

[1]Cornell University, Center for Radiophysics and Space Research, Department of Astronomy, Ithaca, New York.
[2]U.S. Geological Survey, Branch of Astrogeology, Flagstaff, Arizona.
[3]Jet Propulsion Laboratory, California Institute of Technology, Pasadena, California.
[4]NASA Ames Research Center, Space Science Division, Moffett Field, California.
[5]Deceased, June 13, 1994.
[6]Lowell Observatory, Flagstaff, Arizona.

Copyright 1996 by the American Geophysical Union.

Paper number 96JE00689.
0148-0227/96/96JE-00689$09.00

showed that atmospheric temperatures could be cold enough for CO_2 cloud condensation at high polar latitudes. Further, *Paige and Ingersoll* [1985] used a one-dimensional polar radiative model to show that if dust or water ice particles are present in the atmosphere, CO_2 cloud condensation is even more likely because the aerosols increase the infrared emissivity of the atmosphere. More recently, *Pollack et al.* [1990b] developed a full three-dimensional GCM simulation of the Martian polar atmosphere, including dust and topographic effects. They found that CO_2 clouds form in the winter polar regions regardless of the dust opacity, but that the rate of CO_2 cloud condensation increases sharply as the dust content increases. Major implications of the *Pollack et al.* [1990b] study were that a substantial fraction of the polar hood (and other) clouds may be composed of CO_2 ice, and that these clouds might play an important role in the transport and removal of atmospheric dust and water, especially in the northern polar regions [e.g., *Paige,* 1989; *Pollack et al.*, 1990b]. In addition, the results of *Kasting* [1991] indicate that CO_2 cloud condensation may limit the magnitude of any early Mars CO_2/H_2O greenhouse. This finding has caused considerable distress among researchers trying to find ways in which Mars could have evolved from an earlier, more clement climate to its current one [e.g., *Haberle et al.*, 1994], and it serves to emphasize the potential importance of continued studies of the Mars CO_2 cycle and of CO_2 clouds in particular.

Direct observational evidence of CO_2 clouds on Mars was reported from Mariner 6 and 7 infrared spectrometer (IRS) limb scans [*Herr and Pimentel,* 1970]. Three of the limb spectra showed a reflection spike at 4.26 μm that was attributed by the IRS team to the strong ν_3 band of solid CO_2, occurring at a height of 25±7 km and at an atmospheric temperature of 130°K. Confirmation of such low equatorial upper atmosphere temperatures was not provided by the Viking infrared thermal mapper (IRTM) observations, however. Indirect evidence of CO_2 clouds comes from (1) Mariner 9 photographs and infrared interferometer spectrometer (IRIS) temperature profiles of north polar hood clouds that were interpreted as indicating that the clouds were composed of H_2O ice at lower latitudes and CO_2 ice at higher latitudes [*Briggs and Leovy,* 1974; *Hanel et al.*, 1972; *Conrath et al.*, 1973]; (2) modeling of Mariner 9 television limb profiles [*Anderson and Leovy,* 1978]; (3) Analysis and modeling of Mariner 9 and Viking global cloud observations [*Kahn,* 1984]; and (4) Viking IRTM brightness temperature observations, indicating anomalously low temperatures (128°K to 134°K) in the polar regions [e.g., *Kieffer et al,* 1976; *Palluconi,* 1977]. Possible explanations for the anomalous IRTM temperatures included low surface emissivities, a lowering of the frost point temperature because of lower CO_2 surface pressure, and CO_2 clouds (see reviews by *Paige* [1989] and *James et al.* [1992]). Both the IRIS and IRTM data sets were critically reexamined recently by *Forget et al.* [1995], who presented evidence that either thick, precipitating CO_2 clouds with significant H_2O ice contamination or millimeter-sized surface CO_2 ice deposits with minor dust and H_2O ice contamination are the causes of the IRTM and IRIS polar temperature anomalies.

Bell et al. [1993] presented the first direct ground-based telescopic evidence for Martian CO_2 ice clouds. Here, we expand upon that preliminary study and present a method for the future detection and monitoring of Martian CO_2 clouds using telescopic or spacecraft infrared imaging spectroscopic techniques. Our primary goal was to try to confirm the previous direct observations of CO_2 clouds on Mars and to determine the optimum detection techniques. Secondary goals were to determine the spatial extent, temporal variability, and composition (H_2O versus CO_2) of any clouds detected, and to use radiative transfer modeling to simulate the telescopic data and to determine the mean particle size and optical depth of polar hood clouds for assessing their role in the polar heat budget. To achieve all of the secondary goals requires an accurate flux calibration of the data, which was unfortunately not possible for the measurements presented here.

In this paper we first discuss the data acquisition and analysis techniques that best optimize the detectability of CO_2 clouds and other Martian volatiles, then we describe the observations that were made during the 1990 and 1993 oppositions. We then present an analysis of our 1990 and 1993 images, including some new radiative transfer modeling results on the detectability of specific CO_2 ice cloud absorption features. Finally, we conclude with a discussion of the implications of the available data on the Martian CO_2 cycle and the ways in which future observations and improved calibrations can best be used to constrain the current (and possibly past) Mars global climate and energy balance.

Detection Technique

We sought to develop a reliable observational technique to detect and map CO_2 clouds on Mars, and, more specifically, to be able to distinguish these clouds from water ice clouds. To begin, we examined the database of the many previous, extensive laboratory studies of H_2O and CO_2 ices and frosts [e.g., *Kieffer,* 1970; *Fink and Sill,* 1982; *Warren,* 1982, 1986; *Cal-*

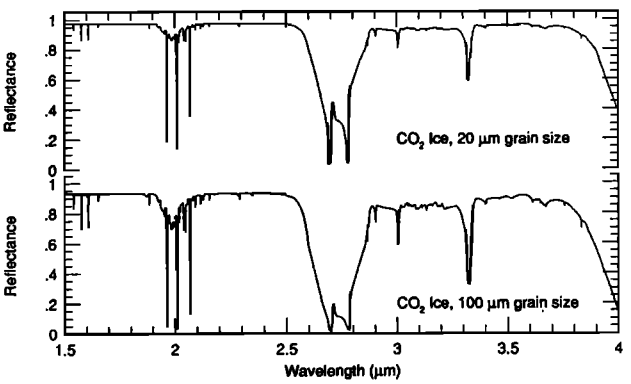

Figure 1. (a) High-resolution near-IR spectra of CO_2 ice at 20-μm and 100-μm grain sizes. These spectra have been calculated using the *Hapke* [1981] model as described by *Calvin and Martin* [1994]. CO_2 ice optical constants were obtained from *Warren* [1986] and *Hansen* [1992] and were adjusted in the 3-μm region using values from *Calvin* [1990]. The spectral resolution of these data ranges from $R = \lambda/\Delta\lambda = 15{,}000$ at 1.5 μm to $R = 400$ at 4.0 μm. (b) Near-IR spectra of coarse- and fine-grained H_2O frost and CO_2 frost compared to a Mars south polar cap spectrum, a Mars atmospheric spectrum, and a terrestrial atmospheric spectrum. All the spectra have been convolved to a resolution matching that of our telescopic data (R = 50 to 70). The H_2O frost data have been calculated from optical constants using a Hapke model as described above. The CO_2 frost data are from *Fink and Sill* [1982]. The Mars polar cap spectrum was obtained by the Mariner 7 spacecraft [*Calvin and Martin,* 1994]. The Mars and Earth model atmospheres are from *Bell et al.* [1994].

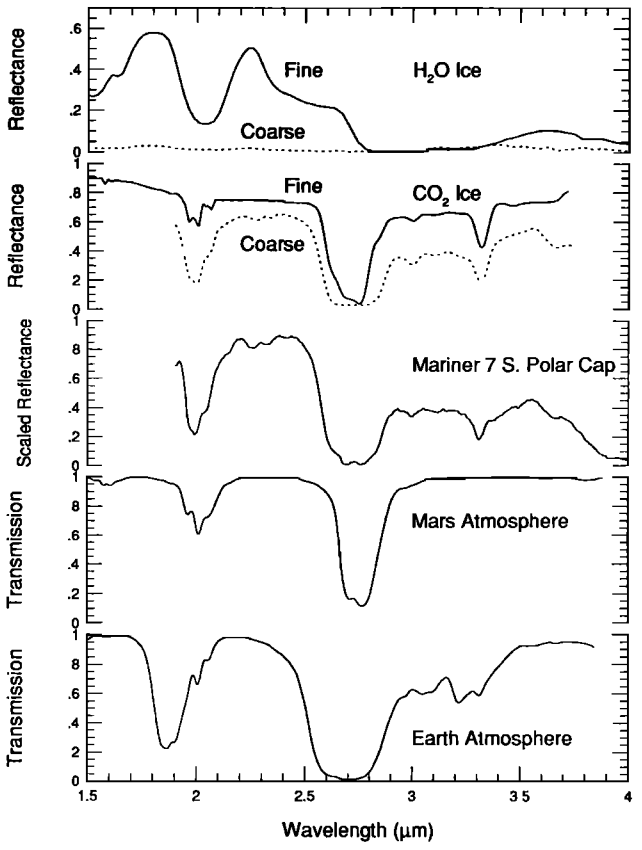

Figure 1. (continued)

vin, 1990; *Hansen,* 1992, 1995]. Our analysis of those data revealed a set of diagnostic absorption features in the near-infrared that can be used to detect and distinguish between H_2O and CO_2 clouds.

Figure 1 shows examples of some representative H_2O and CO_2 ice spectra, as well as Mars surface and modeled Mars and Earth atmospheric spectra. CO_2 ice spectra are shown at high spectral resolution in Figure 1a in order to demonstrate the substantial amount of fine structure in the spectra of solid CO_2. This fine structure is absent in high-resolution H_2O ice spectra because the solid H_2O bands are so broad. In Fig. 1b the spectra are shown at a spectral resolution comparable to that of our telescopic observations. In the visible to near IR, both H_2O ice and CO_2 ice are very bright and difficult to distinguish spectrally. Between 1.5 and 4.0 μm, however, distinct features emerge. In particular, four wavelength regions provide the best spectral discrimination (Table 1): (1) near 2.04 μm, where at low to moderate spectral resolution, water ice has a strong, broad feature and CO_2 ice has weaker, narrower bands; (2) near 2.30 μm, where coarse-grained CO_2 ice has several distinct absorption features not seen in the spectra of water ice or fine-grained CO_2 ice [*Calvin and Martin,* 1994]; (3) near 3.0 μm, where the water ice reflectance is extremely low because of the strong, broad overtone of the fundamental H_2O band but where the CO_2 ice reflectance is high and only a narrow, weaker band is seen; and (4) near 3.33 μm, where CO_2 ice has a strong, relatively narrow absorption feature and where water ice re-

Table 1. Primary Near IR Wavelength Regions for the Detection and Discrimination of H_2O and CO_2 Ices

Region	Range, μm	Justification
1	1.78 to 2.14	Strong, broad 2-μm H_2O ice band; weaker, narrower 2-μm CO_2 ice bands
2	2.25 to 2.37	Narrow CO_2 ice bands in coarser samples
3	2.94 to 3.07	Strong, broad 3-μm H_2O ice band; weak or no CO_2 ice band
4	3.24 to 3 38	Strong, narrow 3.33-μm CO_2 ice band; H_2O uniformly dark

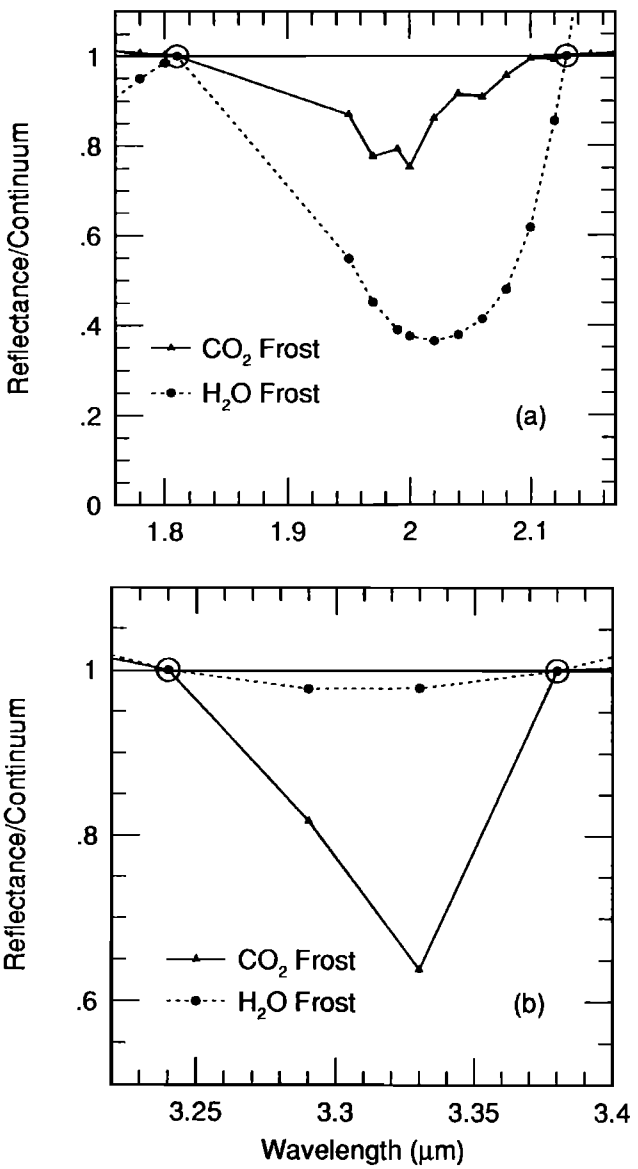

Figure 2. Continuum-removed spectra of H_2O frost (dashed line) and CO_2 frost (solid line) shown in Figure 1. This figure displays two spectral segments where absorption features occur that are diagnostic of these two ices. Within each spectral segment, a linear continuum has been fit between the points indicated with open circles, and then divided from the data. Relative band depth for these pure ice spectra is determined at each of the wavelengths of our telescopic images (solid points) by taking 1.0 minus the y axis value within each segment. This is the same technique that is used for the images in this study, derived from the relative band depth mapping algorithm of *Bell and Crisp* [1993].

mains strongly absorbing. In addition, laboratory studies have shown that the overall reflectance level in the near IR, for example, near 3.60 μm, can be used in well-calibrated data to discriminate between coarse- and fine-grained water ice [e.g., *Roush et al.*, 1990]. We have chosen to concentrate our cloud detection and monitoring efforts on the four near IR spectral regions listed above; calibration uncertainties in the data discussed here have prevented us from using the absolute reflectance level as a way to discriminate the H_2O ice grain size. As can be seen in Figure 1, the Martian surface and atmosphere, and the Earth's atmosphere (for ground-based observations) also introduce spectral features in the near IR that must be considered when analyzing the data.

The detection technique we decided on was telescopic multispectral imaging at low to moderate spectral resolution and at the highest possible spatial resolution. The procedure was to obtain images in the four diagnostic spectral regions (and adjacent continuum), and then spatially co-register the images into a three-dimensional multispectral image cube. Then, relative band depth (RBD) mapping techniques or color ratio images were used to analyze the data [e.g., *Bell and Crisp*, 1993]. Figure 2 demonstrates how a careful choice of continuum and in-band imaging wavelengths can be used to maximize the potential for detection of absorption features using RBD.

Observations and Data Reduction

Near-infrared multispectral images of Mars were obtained from the NASA 3.0-m Infrared Telescope Facility (IRTF) at Mauna Kea Observatory, Hawaii. The images were obtained using the ProtoCAM 58×62 InSb array camera and its cooled circular variable filter (CVF) at a spectral resolution of 0.9% to 1.4% ($\Delta\lambda/\lambda$). Observations were made during November 15-17, 1990 UT and on January 12, 1993 UT. The 1990 data were obtained 2 weeks before opposition, when Mars subtended 18 arc sec and was at a phase angle of 12° and L_S=333° (mid northern winter). The maximum sub-Earth point spatial resolution of these images (at a 0.35 arc sec/pixel scale) is ≈ 130 km. More than 800 Mars images were obtained during this time, but only about 80 at the most diagnostic wavelengths were used for this study (see *Bell and Crisp* [1993] for details). The 1993 data were obtained 5 days after opposition when Mars subtended 15 arc sec and was at a phase angle of 4° and L_S=25° (mid northern spring). Maximum spatial resolution in these images (at 0.30 arc sec/pixel scale) is ≈ 160 km. Thirteen images at three diagnostic wavelengths were obtained during 1993 (Table 2).

Data collection and reduction procedures for the 1990 images were described in detail by *Bell and Crisp* [1993]. The same procedures were applied to the 1993 images. Briefly, this involved the acquisition of additional bias, dark current, and flat-field images and the application of standard image linearization procedures to remove instrumental effects and arrive at a linear relationship between observed pixel values and Mars flux. The instrumental signal-to-noise ratio (SNR) for the 1990 data after processing ranged from 200 to 400 [*Bell and Crisp*, 1993]. The 1993 images have higher instrumental SNR values (600 to 1200) because multiple integrations were used and then coadded to obtain each image (Table 3). The actual SNR of these images is constrained not by instrumental SNR, but by systematic errors resulting from telescope tracking accuracy, wind shake, and telluric atmospheric variations. The analyses performed below indicate that these systematic errors limit the effective SNR to about 100, meaning that relative spectral variability below the 1% level must be interpreted with caution.

Because of nonphotometric weather conditions for the 1990 data and the lack of sufficient observing time for the 1993 data, the images could not be calibrated into absolute flux using standard stars. Comparisons with radiative transfer modeling results were thus made in a qualitative sense only. However, the relative calibration and analysis techniques that we used on the data (such as RBD [*Bell and Crisp*, 1993]) do not require an absolute spectrophotometric calibration.

Results and Analyses

Detection of Clouds in the Near Infrared

Our experience has shown that the simplest way to search for evidence of thin polar or limb clouds in near IR Mars images is to make color ratios of images at wavelengths between 2.2 and 3.3 μm. Near 2.25 μm, Mars has a reflectivity maximum [e.g., *Roush et al.*, 1992; *Bell et al.*, 1994], the Martian atmosphere has only very weak (≈ 1%) CO_2 and CO absorption bands [*Crisp*, 1990], and both H_2O and CO_2 ices have relatively high reflectivity (Figure 1). Thus images near 2.25 μm serve as excellent continuum indicators. Near 3 μm, the Martian surface reflectance is lower because of the presence of hydrated minerals and the H_2O ice reflectance is very low, but the CO_2 ice reflectance is still relatively high (Figure 1). Examples of such ratio images from 1990 and 1993 are shown in Figure 3. Because of increased Mars atmospheric absorption, both the 1990 and 1993 data sets are limb darkened at the longer wavelengths, resulting in the bright appearance of the limb in the Figure 3b short λ / long λ ratios [*Bell and Crisp*, 1993]. Other features are visible, however, that are not due to limb effects. In the 1990 2.25/2.94 μm ratio image, most of the north polar region above 50°N shows an enhanced ratio value, as does a much smaller region poleward of 70°S. In the 1993 2.42/3.02 μm ratio image, both polar regions again show enhanced ratio values, but the extent appears to be greater in the south (below 45°S) than in the north (above 50°N). The enhanced ratio values (derived from the data number (DN) levels in the bias, sky, and flat-field corrected im-

Table 2. Observational Circumstances of IRTF Mars Images from January 12, 1993 UT

Wavelength, μm	Number of Images	Time, UT	Exposure, s	SE Latitude, deg	SE Longitude, deg	SS Latitude, deg	SS Longitude, deg	Phase, deg
2.42	5	1218	0.2	6.50	76.72	10.43	74.14	4.6
3.02	4	1212	1.0	6.50	75.25	10.43	72.68	4.6
3.33	4	1214	1.0	6.50	73.17	10.43	73.17	4.6

SE = Sub-Earth; SS = Sub-Solar.

Table 3. Instrumental Signal to Noise (S/N) of 1993 IRTF Mars Images

Image	λ, μm	Coadds	Raw Data, × 10^3 e^- Object B	Object D	Sky	Noise, e^- B	Noise, e^- D	S/N Value After Processing Step 1 B	Step 1 D	Step 2 B	Step 2 D
Representative Values for Bright and Dark Surface Regions											
092	2.42	2	1787	677	8	1423	956	1250	700	840	596
070	3.02	2	1899	878	62	1443	1030	1273	792	1090	742
078	3.33	2	2401	1040	246	1549	1019	1391	779	1214	744
Flat-Field Images											
342	2.42	3	1799		214	1397		1135			
339	3.02	10	8390		2950	2582		2106			
341	3.33	20	14255		6205	3240		2485			

All data from images obtained on January 12, 1993 UT. Instrumental noise in raw (unprocessed, uncalibrated) images is $(P^2+R^2)^{0.5}$, where P is photon noise = (Object - Sky)$^{0.5}$ and R is read noise ≈ $350N^{0.5}$ e^-, where N is the number of coadds used to obtain the data. Instrumental gain is 50 e^-/DN. B, bright region; D, dark region. Step 1 is the S/N value after subtraction of the sky signal from the object signal. Step 2 is the S/N value after flat-field correction of the Mars images. Errors calculated using standard error propagation formulae [e.g., *Bevington*, 1969].

ages) range from 1.9 to 4.2, a factor of 2 to 4 above the equatorial region ratio values. The spatial location and spectral behavior of the enhanced ratio features in Figure 3b strongly suggest that they are caused by water ice, rather than CO_2 ice, based on an analysis of the spectra in Figure 1. The region of enhanced 3.0 μm absorption also correlates well with the region of high UV brightness observed in Hubble space telescope (HST) images of Mars obtained in December 1990 at L_S=349° [*James et al.*, 1994]. However, the HST data cannot distinguish between H_2O or CO_2 ice as the cause of the high UV cloud and polar surface brightness.

The 3.33/3.02 μm ratio images from 1990 and 1993 (Figure 3c) also show interesting and diagnostic spatial structure that is different from that in Figure 3b. The 1990 3.33/3.02 μm ratio image shows enhanced values at both poles, but the effect is restricted to higher latitudes than in Figure 3b. The 1993 3.33/3.02 μm ratio shows a strongly enhanced feature in the south polar region but only a very weak feature in the northern high latitudes. There is a distinct correlation between albedo (Figure 3a) and ratio value above 30°N in Figure 3c. This correlation, as well as the appearance of other features at low and middle latitudes in these ratio images, argues against a surface ice or atmospheric ice origin for some of the high northern latitude ratio image features. However, certain other features, such as the bright bands at 60°N and 75°S and the dark band at 50°N in the 1990 ratio and the bright region south of 45°S in the 1993 ratio, are clearly related to polar volatiles. Inspection of the spectra in Figure 1 indicates that bright regions in Figure 3c may correspond to areas that have a 3.02-μm (H_2O ice) absorption feature that is stronger than any 3.33-μm (CO_2 ice) absorption feature. Conversely, darker regions may indicate enhanced CO_2 ice.

It is difficult to uniquely interpret the results in Figure 3, however, because factors such as surface albedo, topographic variations, and aerosol opacity can strongly influence the spectral slope between two wavelengths [e.g., *Bell and Crisp*, 1993]. Thus, while the spatial and spectral variability ob-

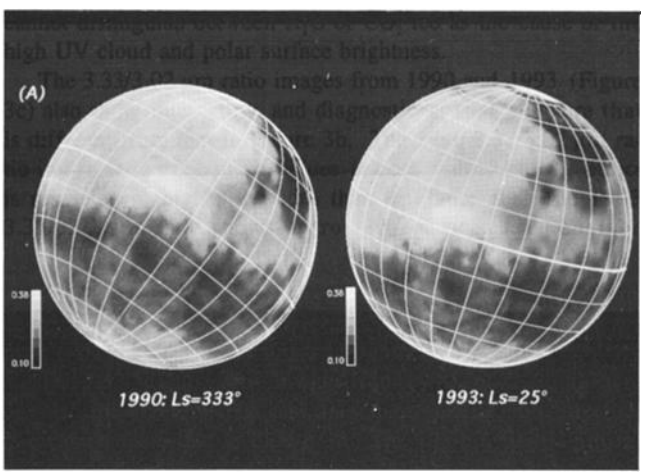

Figure 3a. Broad-band visible albedo from the Viking IRTM data set displayed in an orthographic projection to simulate the viewing geometry at the time that our 1990 and 1993 near IR images were obtained. Grid lines are spaced at 15° intervals, and the equator is marked by the heavy line. The sub-Earth point for the 1990 image is at 6.6°S, 77.9°W, and the sub-Earth point for the 1993 image is at 6.5°N, 76.0°W.

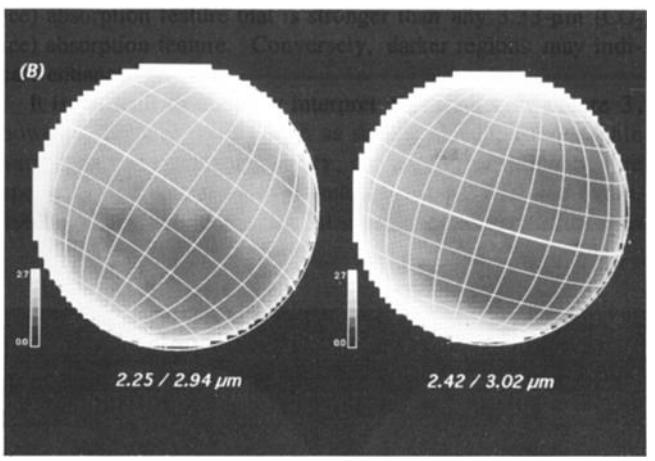

Figure 3b. The 2.25/2.94 μm ratio from 1990 data (left), and the 2.42/3.02 μm ratio from 1993 data (right). The ratio values represent ratios of data numbers (DNs) from reduced images (bias, sky, flat-field corrected), not ratios of reflectances.

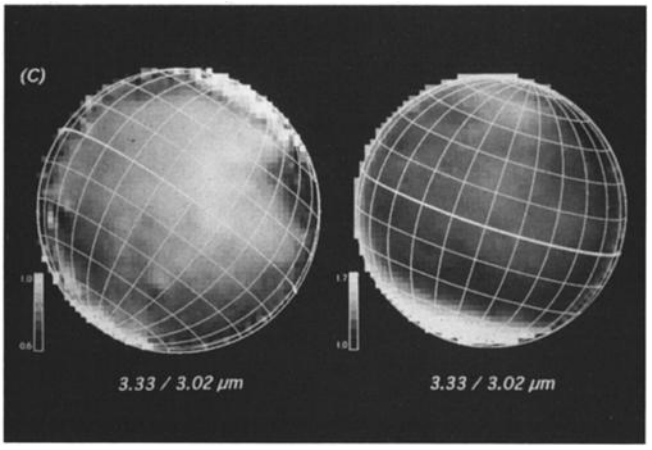

Figure 3c. The 3.33 / 3.02 μm ratio from 1990 (left) and 1993 (right). Again, ratio values are from reduced DN ratios, not ratios of reflectances.

served in Figures 3b and 3c is interesting and indicative of the presence of polar volatiles, the ratio image technique is not an optimum method for the unique compositional discrimination of the materials responsible for the observed variability.

Evidence for Specific Absorption Features

More diagnostic information on the strength and spatial distribution of specific absorption features can be obtained with RBD mapping techniques [*Bell and Crisp,* 1993]. Figure 4 presents RBD mapping results for 1990 data in each of the four wavelength intervals in Table 1. Two different central wavelengths were chosen from each of the four intervals, but the same continuum points were used for each of the intervals' two central wavelengths. Many of these RBD maps show evidence for spectral variability in the north polar regions of Mars. The spatially contiguous nature of the variability, especially of features that fall along lines of constant latitude, indicates that misregistration or other data reduction artifacts are not responsible for this variability.

The maps in Figure 4 can be interpreted using the spectra in Figures 1 and 2 as a guide. For example, Figure 4a, which is a map of 2.00-μm band depth relative to a linear continuum between 1.81 and 2.13 μm, shows increased absorption at high northern latitudes. Examination of the Mars atmospheric spectrum in Figure 1 and comparisons with Mars topography data and the results from *Bell and Crisp* [1993] reveal that some of this variability is caused by atmospheric CO_2 pathlength variations. Figure 2a indicates that at 2.00 μm, any fine-grained H_2O ice that is present will have a much more dominant spectral effect than fine-grained CO_2 ice. At 2.10 μm (Figure 4b), atmospheric CO_2 absorption is much weaker and CO_2 ice does not show any substantial absorption. H_2O ice, however, would still be strongly absorbing at this wavelength relative to the continuum points used. The lesser evidence for strong polar absorption at 2.10 μm (Figure 4b) therefore indicates that the polar absorption seen at 2.00 μm (Figure 4a) is probably due to either atmospheric CO_2 (topographic variations) or CO_2 ice. This reasoning also suggests that the strongly absorbing polar material in the 3-μm ratio images of Figure 3b is H_2O ice, either the north polar cap itself or high latitude "polar hood" water ice clouds. The data of Figures 4a and 4b are perhaps more consistent with the origin of the 3-μm absorption as coarse-grained surface ice because if the absorbing material were fine-grained H_2O ice, similarly strong absorption would be expected to be seen at both 2.00 and 2.10 μm (Figures 4a and 4b).

Band depth maps in the 2.30-μm region (Figures 4c and 4d) are sensitive to coarse-grained CO_2 ice features (Figure 1 [*Calvin and Martin,* 1994]), and also to weak surface mineralogic features [e.g., *Clark et al.,* 1990; *Bell and Crisp,* 1993; *Murchie et al.,* 1993; *Bell et al.,* 1994]. While both maps in the 2.30-μm region show evidence for interesting spatial variability at equatorial and mid latitudes, neither show any firm evidence for increased absorption at polar latitudes resembling the absorption seen in Figures 4a and 4b. The origin of the weak features that do exist in these images is the subject of a separate investigation.

Near 3 μm the band depth maps do show structure in the polar regions, with the higher SNR occurring in the 3.02 μm map (Figure 4f). Both the 2.98 μm map (Figure 4e) and the 3.02 μm map show evidence for a band at 45°N to 50°N that exhibits a 3-μm feature that is from 3 to 10% weaker than the disk-averaged 3-μm band. Despite the fact that pure fine-grained H_2O ice should show a strong absorption in these images if present (Figure 1), there is little evidence for regions exhibiting stronger 3-μm band depth than the disk averaged values. Fine-grained CO_2 ice, if present, would probably not be detectable in these maps at the SNR of our data. In fact, radiative transfer modeling results, discussed below, indicate that RBD maps in the 2.98- to 3.02-μm region are not very sensitive to CO_2 ice, and in fact the "negative" band depth feature seen in Figures 4e and 4f may be related to a surface, rather than atmospheric, effect.

Finally, in the 3.3-μm region, there is again evidence of spatially contiguous spectral variability in the north polar region. At 3.29 μm (Figure 4g), another dark band of lower-than-average band depth appears at constant latitude, but this band is located approximately 5°-10° north (at 50°N-60°N) of the band seen in the 2.98-μm and 3.02-μm RBD images. The origin of this dark band is uncertain. At 3.33 μm (Figure 4h), where any evidence for CO_2 ice would be strongest (Figure 2b), the RBD image shows a region of enhanced band depth north of 60°N, at higher latitudes than either of the dark bands seen in previous figures. The bright regions in Figure 4h, which occur only at the highest visible northern latitudes, provide our best evidence for the detection of fine-grained CO_2 ice clouds in these data. Fine-grained H_2O ice clouds or coarser-grained surface H_2O ice, if present, should not show enhanced band depth in such an image (Figure 2b). We do not believe that this feature is due to coarse-grained CO_2 ice because there is no evidence for similar absorption at wavelengths that can much more uniquely identify coarse-grained CO_2 ice (Figures 4c and 4d). However, the coarse-grained CO_2 ice features could be masked by minor contamination by water ice or dust, or could be reduced in contrast by particle size or emission angle effects. Thus our interpretation of fine-grained CO_2 ice clouds as the origin of the features in Figure 4h is not definitive.

Radiative Transfer Modeling Simulations

We have used a radiative transfer model to try to simulate the near IR spectral behavior of Mars ice clouds and to try to understand the magnitude of the spectral variability that we can expect to see in our data under a variety of circumstances. For

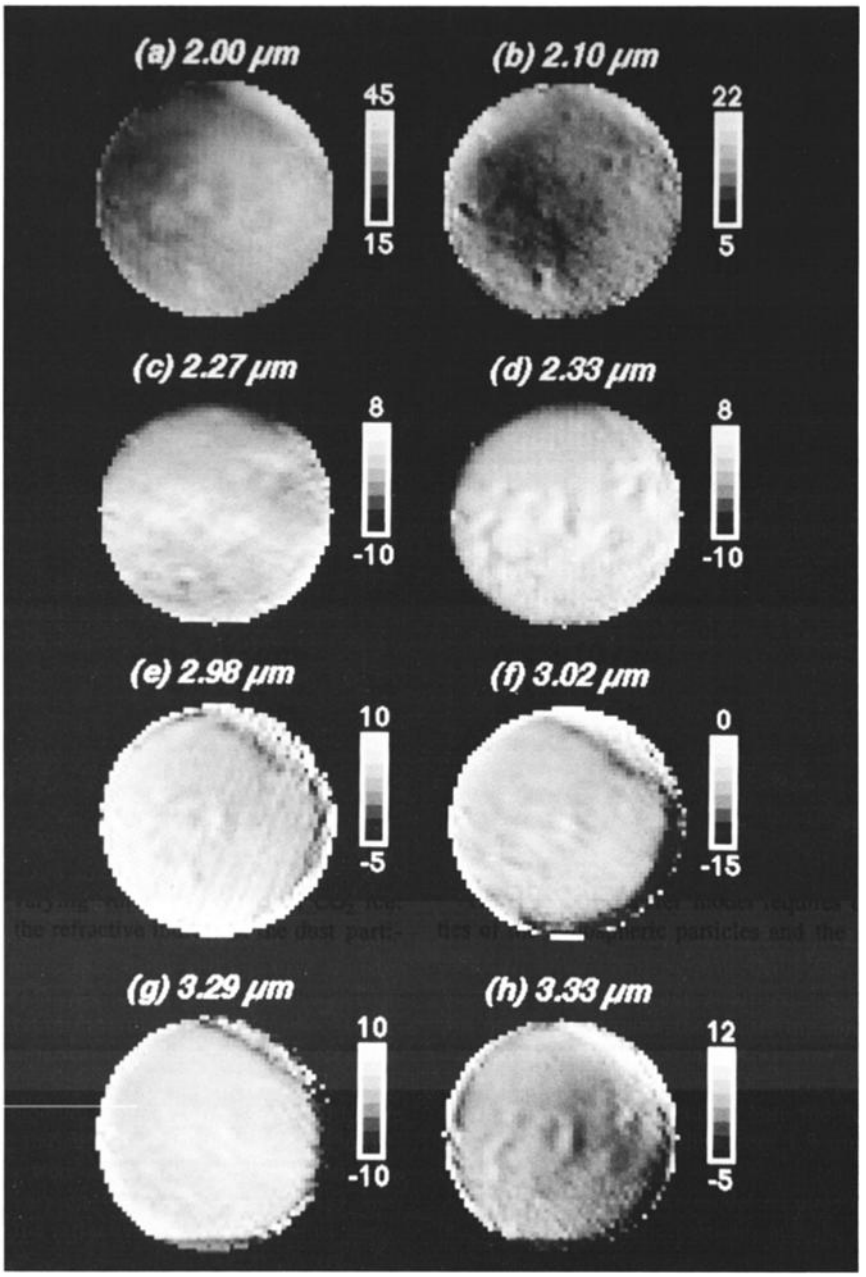

Figure 4. Relative band depth mapping results for two images in each of the four intervals shown in Figure 2. (a) 2.00 μm relative to a linear continuum between 1.81 and 2.13 μm; (b) 2.10 μm, continuum points 1.81 and 2.13 μm; (c) 2.27 μm, continuum points 2.21 and 2.40 μm; (d) 2.33 μm, continuum points 2.21 and 2.40 μm; (e) 2.98 μm, continuum points 2.94 and 3.07 μm; (f) 3.02 μm, continuum points 2.94 and 3.07 μm; (g) 3.29 μm, continuum points 3.24 and 3.38 μm; (h) 3.33 μm, continuum points 3.24 and 3.38 μm. The RBD values shown in the scale bars are in percent.

this preliminary analysis, we modeled only CO_2 ice clouds overlying a typical bright region, using the radiative transfer technique described by *Pollack et al.* [1995]. This model includes a Hapke representation for the surface [*Hapke,* 1981, 1993] and a Mie or nonspherical particle scattering representation for the atmospheric scatterers. The atmosphere is modeled using the doubling method, and the surface is added to the atmosphere system using the adding method [*Hansen,* 1969].

The ice cloud particles were assumed to be composed of a dust core surrounded by varying volume fractions of CO_2 ice. In order to achieve this, the refractive indices of the dust particles [*Ockert-Bell et al.,* 1995] and those of CO_2 ice [*Calvin,* 1990; *Hansen,* 1995] were needed. The cloud particles are assumed to be spherical and stratified. A Mie scattering method was used to determine the scattering properties of combined dust/ice particles [*Toon and Ackerman,* 1981]. Ice shell volume fractions of 30, 60, and 90% were tested. In this case the shell fraction is simply added onto the dust particle, increasing the particle effective radius from 1.8 μm (no ice) to 3.5 μm (90% shell).

The radiative transfer model requires the scattering properties of the atmospheric particles and the surface, the geometry

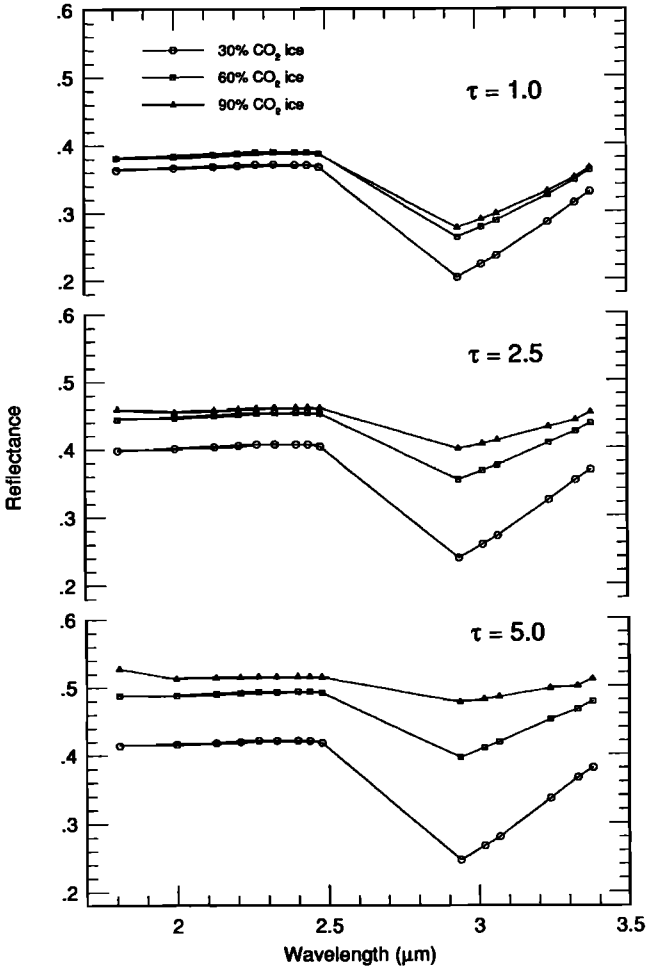

Figure 5. Reflectance spectra at 15 diagnostic near IR wavelengths derived from a radiative transfer model simulation of stratified CO_2 ice cloud particles overlying a typical bright surface region. The particles are composed of a bright dust core and varying volume percentages of an overlying CO_2 ice shell. Three different 2-μm cloud opacity cases were considered. Note the small effect of the cloud particles on the reflectance at low opacity, and the dramatically increasing effect of increasing the CO_2 ice shell percentage at higher cloud opacity values.

of the observation, and an optical depth. For the surface optical constants, we used the dust optical constants that were derived by *Ockert-Bell et al.* [1995] under the assumption that bright surface regions and airborne dust have similar properties. We assumed a constant geometry appropriate for observations from Earth of high latitudes on Mars (incidence angle = emission angle = 55°. phase angle = 5°). Three optical depths (τ) were chosen: 1.0, 2.5, and 5.0 (τ at 2.0 μm). The model was run at 15 near IR wavelengths, chosen because they match the wavelengths of our telescopic data, which were designed to optimize the detection of CO_2 and H_2O ice features. Because optical depth is linearly dependent on the extinction coefficient of the scatterer, which in turn is dependent on wavelength, the 2.0-μm optical depths chosen above were scaled appropriately for other wavelengths.

Results from this model are shown in Figure 5. For low cloud opacities and/or low ice to dust ratios, the model reflectance deviates very little from the reflectance of the bright underlying surface [e.g., *Mustard and Bell,* 1994]. As the cloud opacity or ice to dust ratio increases, however, the spectral effects of the CO_2 ice become more apparent. Specifically, the reflectance increases, the strength of the 3-μm hydrated minerals band decreases, and features in the 2.0- and 3.3-μm regions (Figure 1) begin to manifest themselves in the data. In Table 4, the relative band depths are calculated for these model spectra in each of the spectral regions shown in Table 1. Band depths were calculated using the same technique and continuum points as for the telescopic data in Figure 4, so that a qualitative relative comparison between the model results and the actual data can be made.

Table 4 shows that there is an increase in RBD value with increasing CO_2 ice shell percentage for all values of τ. However, the 2.00- and 3.33-μm bands exhibit substantially higher RBD values than the 2.33- and 3.02-μm bands, even at low opacities and low CO_2 ice shell percentage. The results in Table 4 indicate that the lower 2.33- and 3.02-μm RBD values are probably due to spectral features in the dust component rather than the ice component. For example, the 2.33-μm band always exhibits a negative RBD value, and even though the value becomes larger with increasing CO_2 ice shell percentage, the CO_2 ice band at 2.33 μm is too weak to drive the RBD to positive values (the 2.33-μm feature is much stronger in coarse-grained CO_2 ice spectra). In contrast, the 3.33-μm RBD values start near zero or negative values for the low-ice cases and then increase dramatically with increasing ice percentage.

The results of this simplified model indicate that CO_2 ice absorption features in the near IR are in fact detectable in a cloud of modest opacity overlying a typical bright surface. These results are also consistent with Figures 1 and 2, in that they indicate that the 2.00-μm and 3.33-μm regions are the best near IR wavelengths at which to search for evidence of CO_2 ice cloud absorption. Although there are weak CO_2 bands at other wavelengths, the detectability of these weaker features is a function of CO_2 ice grain size and also can be hampered by the presence of surface mineral absorption features of comparable strength.

Table 4. Relative Band Depths for a Modeled CO_2 Cloud Overlying a Bright Surface Region

Wavelength,	τ = 1.0			τ = 2.5			τ = 5.0		
μm	30%	60%	90%	30%	60%	90%	30%	60%	90%
2.00	-0.003	0.074	0.324	0.042	0.190	0.771	0.090	0.324	1.322
2.33	-0.265	-0.222	-0.252	-0.188	-0.151	-0.119	-0.149	-0.074	-0.050
3.02	-0.024	0.000	0.098	-0.107	-0.057	0.047	-0.104	-0.081	0.021
3.33	0.014	0.433	0.625	-0.191	0.445	0.827	-0.329	0.508	1.086

Band depth values are in percent; τ = 2-μm opacity. Values are shown for particles with CO_2 ice shells of 30%, 60%, and 90% by volume.

Discussion

Why Clouds?

While it is clear that absorption features caused by H_2O and CO_2 ices have been detected in our data, it is less obvious that these features are due to clouds rather than surface ice deposits (the polar caps). Several pieces of evidence lead us to believe that clouds have been detected in these data and that they can be discriminated from the polar caps. The first piece of evidence comes from the RBD maps of Figures 4a-4d. These maps show evidence for absorption by CO_2 as opposed to H_2O (Figures 4a and 4b) and indicate that the CO_2 is not coarse-grained (Figures 4c and 4d). The spatial extent and strength of the increased polar absorption in Figure 4a are very different from those seen in Figure 3b (ascribed to H_2O ice in the polar cap), also possibly suggesting a different origin. This interpretation is supported by the 3.33-μm RBD map of Figure 4h, which shows evidence for CO_2 ice absorption at high polar latitudes. The 3.33-μm band alone, however, is not able to uniquely discriminate between coarse- and fine-grained CO_2 ice.

The second piece of evidence for the detection of clouds in our near IR data is the lack of a high-albedo polar cap in the images. Figure 1 indicates that at continuum wavelengths below about 2.5 μm a water ice or CO_2 ice polar cap would have a high reflectance, similar to that which would be observed in the visible. No such bright cap is seen in the 1990 near IR data [*Bell and Crisp,* 1993] or in visible CCD images obtained nearly simultaneously [*Bell,* 1991]. HST visible-wavelength images obtained in December 1990 show a UV-bright band at high northern latitudes, but analysis of those data indicates that this band may be caused primarily by clouds rather than surface ice [*James et al.,* 1994]. In late 1990 the observational geometry was such that the north polar region was not visible from Earth (Figure 3a), so it may not have been possible to see much of the late winter polar cap anyway. In 1993 the observational geometry was more favorable in the north (Figure 3a), yet still no clear evidence of a bright surface cap was seen in the near IR images. This point is weakened, however, by recent reanalysis of Viking Orbiter images and IRTM data that indicate possible evidence for clear, solid CO_2 ice deposits that are transparent to visible and infrared radiation [*Paige et al.,* 1995].

A third piece of evidence is the spatial extent of the polar absorptions and the nearly perfect alignment along constant latitudes that could suggest the presence of a mobile, atmospheric material rather than a surface deposit. Determinations of the north polar cap regression versus season [e.g., *James et al.,* 1992, Figure 5] indicate that the absorber causing the near IR features that we have detected in Figures 3 and 4 extends slightly farther south than the likely edge of the surface cap at the appropriate season. However, polar cap growth and regression vary from year to year, so it is not possible to uniquely eliminate the possibility that the cap edge could have been farther south during the particular times of our observations. This possibility is not consistent with the HST data discussed earlier, however.

Finally, additional theoretical support comes from the fact that polar clouds are a common feature on Mars [e.g., *Slipher,* 1962; *Briggs and Leovy,* 1974; *Martin et al.,* 1992], and perhaps the most relevant question for the current study is whether or not it is reasonable to expect CO_2 clouds in particular to be present at the times of our observations. The GCM simulations of *Pollack et al.* [1990b] directly addressed this issue. Pollack et al. found that under some conditions, CO_2 ice clouds should be a ubiquitous feature at the winter poles, with model atmospheric temperatures sometimes dropping below the CO_2 frost point at latitudes as low as 40°. In fact, these authors suggested that the polar hood clouds typically observed from the Mars autumnal to vernal equinoxes may be a manifestation of the high polar atmospheric CO_2 condensation rates predicted by their GCM. Supporting evidence for the presence of CO_2 clouds and of active CO_2 condensation was discussed earlier, and includes the anomalously low and spatially and time variable Viking IRTM 20-μm polar brightness temperatures and the unique spectral character of some of the Mariner 9 IRIS spectra in the polar regions [*Kieffer et al.,* 1976; *Forget et al.,* 1995].

Seasonal Variability: 1990 versus 1993

Although both the 1990 and 1993 near IR imaging data sets are relatively small and sample only a single point in the seasonal cycles of two Mars years, some general statements can be made about the seasonal differences between the data sets. The 1990 data, obtained at L_S=333° (late northern winter), show evidence for condensate activity in both the north and south polar regions, although the scale of the activity is much greater in the winter hemisphere. The limited 1993 data, obtained at L_S=25° (early northern spring, about 15% farther along in the seasonal cycle than the 1990 data), show evidence for cloud activity in both the north and the south, although the scale of the activity appears greater in the south at this time. It was not possible to make the same types of band depth maps for the 1993 data as the 1990 data, so unique compositional distinctions cannot be made. However, the 3.33/3.02 μm ratio images (Figure 3c) show a dramatic change in the spatial distribution of polar clouds in just 50° of (relative) L_S, especially in the southern hemisphere. Without additional coverage at intervening seasons, it is impossible to constrain the detailed style and timing of volatile transport responsible for these observed changes. Nonetheless, these data provide a tantalizing glimpse of the types of information on seasonal variability that could be obtained with more detailed and systematic ground-based or spacecraft observations.

Future Observational and Modeling Studies

The results presented here must be considered only preliminary because the observations have only sparsely sampled a few points in the Mars seasonal cycle. We are currently performing a more focused program from the NASA IRTF of near IR multispectral imaging observations over a wider range of the Mars seasonal cycle (L_S=340° to 80° during the 1994-1995 apparition [*Bell et al.,* 1995]). Other groups, as well, are using facility near IR array cameras to image Mars at key wavelengths [e.g., *Blaney,* 1991; *Klassen et al.,* 1993]. This research would benefit greatly from additional ground-based observational studies, especially at times when Mars is relatively far from opposition. The loss of spatial resolution far from opposition can be at least partly compensated using adaptive optics systems, instruments with variable plate scale capability at excellent sites, or space-based telescopes. In addition, observations at higher spectral resolution may simplify the unique identification of CO_2 ice because CO_2 ice has a number of extremely narrow absorption features in the near IR that are essentially undetectable at low spectral resolution (Figure 1 [*Hansen,* 1995]).

Particularly promising future observational capabilities exist from Earth-orbiting telescopes, such as the planned HST near IR camera and the European Space Agency's Infrared Space Observatory. While it is unlikely that observations from these platforms will improve upon the ability of ground-based telescopes to sample a large range of the Martian year, the substantial increase in spatial resolution will allow much more detailed information on the spatial variability of near IR absorption features to be obtained, especially at times when Mars is far from opposition. As well, global near IR imaging and spectroscopic observations from Mars-orbiting spacecraft, such as those planned for the NASA Mars Global Surveyor and Russian Mars-96 missions, will allow even higher spatial resolution data to be obtained. Such measurements, if they can be carried out over a full seasonal cycle and if ground-based data can be used to provide a basis for global synoptic monitoring, will substantially increase our understanding of volatile transport on Mars.

Finally, we plan to implement additional refinements and modifications to the radiative transfer model used to derive the results in Figure 5 and Table 4. Specifically, we plan to perform the same analyses for water ice clouds, and then to consider mixes of water ice and CO_2 ice clouds in the model. We also need to consider how the results vary if we use different surfaces underlying the ice clouds. Examples include typical dark region materials, and bright surface water ice and CO_2 ice deposits. The model must also be run at many more wavelengths, not only to allow more realistic comparison with available near IR spectra, but also to allow us to search for other wavelength regions which might yield more diagnostic spectral information that the subset that we have currently chosen for our imaging study.

Conclusions

The major findings of this study are as follows.

1. The observational approach of narrowband multispectral imaging at specific, well-chosen near IR wavelengths is capable of detecting and discriminating CO_2 and H_2O ice clouds on Mars.

2. A simple near IR test for the presence of polar volatiles is to ratio images taken near 2.3 μm to those obtained near 3.0 μm. Polar hood water ice clouds will exhibit substantially enhanced ratio values in such images. Additional images obtained near 3.33 μm can be used for similar ratios, and this wavelength is more likely to reveal the presence of CO_2 ice. However, there are no unique ways to derive cloud or surface ice composition from such simple ratios.

3. Three of the four wavelength regions that we identified as potentially most diagnostic for the mapping of specific, narrow absorption bands reveal spatially confined absorption features in the Mars polar regions. These wavelength regions appear to provide unique, diagnostic compositional information relevant to clouds: at 3.00 μm, where the absorption is dominated by water ice; and at 3.33 μm and 2.00 μm, where the absorption is dominated by CO_2 ice.

4. The results of a simple radiative transfer model simulation of our observational data indicate that the CO_2 ice absorption feature at 3.33 μm should be detectable from a cloud of even low opacity overlying a typical bright surface region. The CO_2 ice features near 2.0 μm should also be detectable, but these features are intermixed with the Mars atmospheric CO_2 spectral signature, which is hard to accurately model in the polar regions. Weaker bands near 2.33 and 3.02 μm do not yield strong, diagnostic bands in the radiative transfer model simulations.

5. Future near IR observational studies that allow Mars images to be obtained over a large fraction of its seasonal cycle will be able to yield useful new information on the rate and style of CO_2 (and H_2O) cloud condensation on Mars. Such data will be useful in more detailed studies and simulations of the Mars polar energy balance [e.g., *Pollack et al.*, 1990b] and for better understanding of the potentially important role of CO_2 clouds in particular. Additionally, further refinements of the radiative transfer simulations of telescopic and spacecraft near IR data are needed in order to more fully understand the origin and implications of the absorption bands that have been detected and mapped.

Acknowledgments. Without the able and enthusiastic cooperation of the NASA IRTF support staff, none of the observations would have been possible. In particular, we thank Mark Shure for patiently guiding us through the vagaries of ProtoCAM observing and data reduction, and Bill Golisch, Dave Griep, and Charlie Kaminski for skillfully operating the IRTF and patiently accommodating our habit of using up every possible moment of precious telescope time. Reviews of an earlier draft of this manuscript by Gary Hansen, Jim Murphy, and Bob Haberle are sincerely appreciated. This work was supported by grants from the NASA Planetary Astronomy (NAGW-3427) and Planetary Geology (RTOP 151-01-60-01) programs. James F. Bell, David Crisp, and John Spencer are visiting astronomers at the Infrared Telescope Facility, operated by the University of Hawaii under NASA contract.

References

Anderson, E., and C. Leovy, Mariner 9 television limb observations of dust and ice hazes on Mars, *J. Atmos. Sci., 35,* 723-734, 1978.

Bell, J.F., III, CCD narrowband filter imaging of Mars during the 1990 opposition (abstract), *Lunar Planet. Sci. XXII,* 71-72, 1991.

Bell, J.F., III, and D. Crisp, Groundbased imaging spectroscopy of Mars in the near-infrared: Preliminary results, *Icarus, 104,* 2-19, 1993.

Bell, J.F., III, W.M. Calvin, J.B. Pollack, and D. Crisp, An observational search for CO_2 ice clouds on Mars (abstract). *Lunar Planet. Sci. XXIV,* 83-84, 1993.

Bell, J.F., III, J.B. Pollack, T.R. Geballe, D.P. Cruikshank, and R. Freedman, Spectroscopy of Mars from 2.04 to 2.44 μm during the 1993 opposition: Absolute calibration and atmospheric vs. mineralogic origin of narrow absorption features, *Icarus, 111,* 106-123, 1994.

Bell, J.F., III, W.F. Golisch, D.M. Griep, C.D. Kaminski, T.L. Roush, and D.R. Klassen, Imaging and spectroscopy of Mars from 1.56 to 4.16 μm: 1994-95 observations from the IRTF (abstract), *Bull. Am. Astron. Soc., 27,* 1091, 1995.

Bevington, P.R., *Data Reduction and Error Analysis for the Physical Sciences.* 336 pp., McGraw-Hill, New York, 1969.

Blaney, D.L., Infrared imaging of Mars between 2.4 and 5.0 μm (abstract). *Lunar Planet. Sci. XXII,* 111-112, 1991.

Blaney, D.L., and T.B. McCord, An observational search for carbonates on Mars, *J. Geophys. Res., 94,* 10,159-10,166, 1989.

Briggs, G.A., and C.B. Leovy, Mariner 9 observations of the Mars north polar hood, *Bull. Am. Meteorol. Soc., 55,* 278-296, 1974.

Calvin, W.M., Additions and corrections to the absorption coefficients of CO_2 ice: Applications to the Martian south polar cap, *J. Geophys. Res., 95,* 14,743-14,750, 1990.

Calvin, W.M., and T.Z. Martin, Spatial variability in the seasonal south polar cap of Mars, *J. Geophys. Res., 99,* 21,143-21,152, 1994.

Clark, R.N., G.A. Swayze, R.B. Singer, and J.B. Pollack, High-resolution reflectance spectra of Mars in the 2.3 μm region: Evidence for the mineral scapolite. *J. Geophys. Res., 95,* 14463-14480, 1990.

Conrath, B.J., R. Curran, R. Hanel, V. Kunde, W. Maguire, J. Pearl, J. Pirraglia, J. Welker, and T. Burke, Atmospheric surface properties

of Mars obtained by infrared spectroscopy on Mariner 9, *J. Geophys. Res., 78,* 4267-4278, 1973.

Crisp, D., Infrared radiative transfer in the dust-free Martian atmosphere, *J. Geophys. Res., 95,* 14,577-14,588, 1990.

Fanale, F.P., and W.A. Cannon, Exchange of adsorbed H_2O and CO_2 between the regolith and atmosphere of Mars caused by changes in surface insolation, *J. Geophys. Res., 79,* 3397-3402, 1974.

Fanale, F.P, S.E. Postawko, J.B. Pollack, M.H. Carr, and R.O. Pepin, Mars. Epochal climate change and volatile history, in *Mars*, edited by H Kieffer et al., pp. 1135-1179, Univ. of Ariz. Press, Tucson, 1992.

Fink, U , and G.T. Sill, The infrared spectral properties of frozen volatiles, in *Comets,* edited by L.L. Wilkening, pp. 164-202. Univ. of Ariz. Press, Tucson, 1982.

Forget, F , G.B. Hansen, and J.B. Pollack, Low brightness temperatures of Martian polar caps: CO_2 clouds or low surface emissivity?, *J. Geophys. Res., 100,* 21,219-21,234, 1995.

Geirasch, P.J , and R. Goody, A study of the thermal and dynamical structure of the Martian lower atmosphere, *Planet. Space Sci., 16,* 615-646, 1968.

Gooding, J L., Soil mineralogy and chemistry on Mars: Possible clues from salts and clays in SNC meteorites, *Icarus, 99,* 28-41, 1992.

Haberle, R M , D. Tyler, C.P. McKay, and W.L. Davis, A model for the evolution of CO_2 on Mars, *Icarus, 109,* 102-120, 1994.

Hanel, R.B., B Conrath, W. Hovis, V. Kunde, P. Lowman, W. Maguire, J Pearl, J. Pirraglia, C. Prabhakara, and B. Schlachman, Investigation of the Martian environment by infrared spectroscopy on Mariner 9, *Icarus, 17,* 423-442, 1972.

Hansen, G.B , The spectral absorption of CO_2 ice from 0.18 to 4.8 μm (abstract), *Bull Am. Astron. Soc., 24,* 978, 1992

Hansen, G.B., The spectral absorption of CO_2 ice from the UV to the far-infrared (abstract), *Bull. Am. Astron Soc., 27,* 1092, 1995.

Hansen, J E., Radiative transfer by doubling of very thin layers, *Astrophys. J , 155,* 565, 1969.

Hapke, B., Bidirectional reflectance spectroscopy, 1, Theory, *J. Geophys Res , 86,* 3039-3054, 1981.

Hapke, B , *Theory of Reflectance and Emittance Spectroscopy,* 455 pp., Cambridge Univ. Press, New York, 1993.

Herr, K.C., and G C. Pimentel, Evidence for solid carbon dioxide in the upper atmosphere of Mars, *Science, 167,* 47-49, 1970.

Jakosky, B.M., and R M Haberle, The seasonal behavior of water on Mars, in *Mars*, edited by H. Kieffer et al., pp 969-1016, Univ. of Ariz Press, Tucson, 1992

James, P B., H.H. Kieffer, and D.A Paige, The seasonal cycle of carbon dioxide on Mars, in *Mars*, edited by H. Kieffer et al., pp. 934-968, Univ. of Ariz Press, Tucson, 1992.

James, P B., R.T Clancy, S. Lee, L J Martin, R.B. Singer, E. Smith, R. Kahn, and R Zurek, Monitoring Mars with the Hubble Space Telescope: 1990-1991 observations, *Icarus, 109,* 79-101, 1994.

Kahn, R., The spatial and seasonal distribution of Martian clouds and some meteorological implications, *J. Geophys. Res , 89,* 6671-6688, 1984.

Kahn, R., The evolution of CO_2 on Mars, *Icarus, 62,* 175-190, 1985.

Kahn, R.A., T.Z. Martin, R.W. Zurek, and S.W. Lee, The Martian dust cycle, in *Mars*, edited by H Kieffer et al., pp. 1017-1053, Univ. of Ariz. Press, Tucson, 1992.

Kasting, J F. (1991) CO_2 condensation and the climate of early Mars, *Icarus, 94,* 1-13

Kieffer, H.H , Spectral reflectance of CO_2-H_2O frosts, *J. Geophys. Res , 75,* 501-509, 1970.

Kieffer, H H., S C Chase Jr., T.Z. Martin, E.D. Miner, and F.D. Palluconi, Martian north pole summer temperatures: Dirty water ice, *Science, 194,* 1341-1344, 1976.

Klassen, D.R , R.R. Howell, and J.F Bell III, Spectral imaging of Mars in the 2-micron region (abstract), *Bull. Am Astron. Soc., 25,* 1034-1035, 1993.

Leovy, C B., and Y. Mintz, Numerical simulation of the atmospheric circulation and climate of Mars, *J. Atmos. Sci., 26,* 1167-1190, 1969.

Martin, L.J., P.B. James, A. Dollfus, K. Iwasaki, and J.D. Beish, Telescopic observations: Visual, photographic, polarimetric, in *Mars* , edited by H.H. Kieffer et al., pp. 34-70, Univ. of Ariz. Press, Tucson, 1992.

Murchie, S., J. Mustard, J. Bishop, J. Head, C. Pieters, and S. Erard, Spatial variations in the spectral properties of bright regions on Mars, *Icarus, 105,* 454-468, 1993.

Mustard, J.F., and J.F. Bell III, New composite reflectance spectra of Mars from 0.4 to 3.14 μm, *Geophys. Res. Lett., 21,* 353-356, 1994.

Ockert-Bell, M.E., C.P. McKay, and J.F. Bell III, The light scattering and absorbing properties of Martian atmospheric dust (abstract), *Bull Am. Astron. Soc., 27,* 1066, 1995.

Paige, D.A., Mariner 9 IRIS and Viking observations of Martian CO_2 clouds, paper presented at Fourth International Conference on Mars, Tucson, Ariz , Jan. 10 to 13, 1989.

Paige, D A., and A.P. Ingersoll, Annual heat balance of Martian caps: Viking observations, *Science, 228,* 1160-1168, 1985.

Paige, D A., D.S. Bass, and S E. Wood, Mars polar caps. Viking evidence for clear solid CO_2 ice (abstract), *Bull. Am. Astron. Soc., 27,* 1098, 1995.

Palluconi, F D , North polar mapping of Mars with the Viking thermal mappers (abstract), *Bull Amer. Astron. Soc., 9,* 540, 1977.

Pollack, J.B., C.B. Leovy, P.W Greiman, and Y. Mintz, A Martian general circulation experiment with large topography, *J. Atmos. Sci., 38,* 3-29, 1981.

Pollack, J B , J.F Kasting, S.M Richardson, and K. Poliakoff, The case for a wet, warm climate on Mars, *Icarus, 71,* 203-224, 1987.

Pollack, J.B , T.L. Roush, F. Witteborn, J. Bregman, D. Wooden, C Stoker, O.B. Toon, D Rank, B. Dalton, and R. Freedman, Thermal emission spectra of Mars (5 4-10.5 μm). Evidence for sulfates, carbonates, and hydrates, *J. Geophys Res., 95,* 14,595-14,627, 1990a.

Pollack, J B., R.M Haberle, J. Schaeffer, and H. Lee, Simulations of the general circulation of the Martian atmosphere, 1, Polar processes, *J Geophys Res., 95,* 1447-1473, 1990b

Pollack, J B., M E Ockert-Bell, and M K. Shepard, Viking Lander image analysis of Martian atmospheric dust, *J. Geophys. Res , 100,* 5235-5250, 1995

Roush, T.L., J B. Pollack, F.C. Witteborn, J.D. Bregman, and J P Simpson (1990) Ice and minerals on Callisto: A reassessment of the reflectance spectra, *Icarus, 86,* 355-382

Roush, T L., E A. Roush, R.B. Singer, and P.G Lucey, Estimates of absolute flux and radiance factor of localized regions on Mars in the 2-4 μm wavelength region, *Icarus, 99,* 42-50, 1992

Slipher, E C., *Mars: The Photographic Story,* 168 pp , Sky Publishing, Cambridge Mass , 1962.

Toon, O B., and T. Ackerman, Algorithms for the calculation of scattering by stratified spheres, *Appl. Opt , 20,* 3657-3660, 1981.

Warren, S G., Optical properties of snow, *Rev. Geophys., 20,* 67-89, 1982.

Warren, S.G , Optical constants of carbon dioxide ice, *Appl Opt., 25,* 2650-2674, 1986.

Zurek, R W , J.R. Barnes, R M. Haberle, J.B. Pollack, J.E. Tillman, and C.B Leovy, Dynamics of the atmosphere of Mars, in *Mars*, edited by H. Kieffer et al., pp. 835-932, Univ. of Ariz. Press, Tucson, 1992

J.F. Bell III and M.E. Ockert-Bell, Department of Astronomy, Center for Radiophysics and Space Research, Cornell University, Ithaca, NY 14853-6801. (email: jimbo@cuspif.tn.cornell.edu; mbell@astrosun.tn.cornell.edu)

W.M. Calvin, Branch of Astrogeology, U.S. Geological Survey, Flagstaff, AZ 86001. (email: wcalvin@hulk.wr.usgs.gov)

D. Crisp, Jet Propulsion Laboratory, California Institute of Technology, Pasadena, CA 91109. (email: dc@crispy jpl.nasa.gov)

J. Spencer, Lowell Observatory, Flagstaff, AZ 86001. (email: spencer@lowell.edu)

(Received November 20, 1995; revised February 21, 1996; accepted February 28, 1996.)